NANO LETTERS

pubs.acs.org/NanoLett Letter

Supramolecular DNA Photonic Hydrogels for On-Demand Control of Coloration with High Spatial and Temporal Resolution

Yixiao Dong, J. Dale Combs, Cong Cao, Eric R. Weeks, Alisina Bazrafshan, SK Aysha Rashid, and Khalid Salaita*

Cite This: https://doi.org/10.1021/acs.nanolett.1c03399 Read Online

ACCESS | Metrics & More | Article Recommendations | Supporting Information

ABSTRACT: Hydrogels embedded with periodic arrays of nanoparticles display a striking photonic crystal coloration that may be useful for applications such as camouflage, anticounterfeiting, and chemical sensing. Dynamically generating color patterns requires control of nanoparticle organization within a polymer network on-demand, which is challenging. We solve this problem by creating a DNA hydrogel system that shows a 50 000-fold decrease in modulus upon heating by ∼10 °C. Magnetic nanoparticles entrapped within these DNA gels generate a structural color only when the gel is heated and a magnetic field is applied. A spatially controlled photonic crystal coloration was achieved by photopatterning with a near-infrared illumination. Color was "erased" by illuminating or heating the gel in the absence of an external magnetic field. The on-demand assembly technology demonstrated here may be beneficial for the development of a new generation of smart materials with potential applications in erasable lithography, encryption, and sensing.

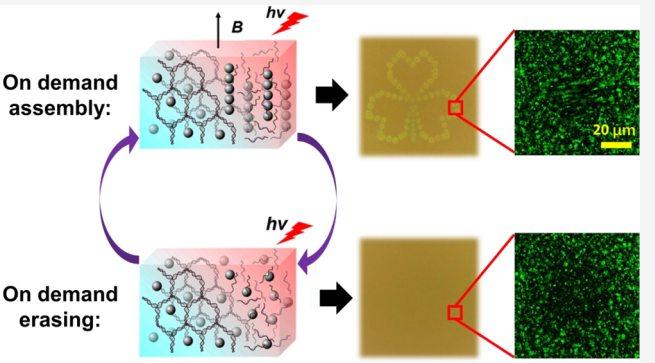

KEYWORDS: *DNA supramolecular hydrogel, photonic crystals, self-assembly, rewritable technology, chromatic response*

INTRODUCTION

Photonic crystals (PCs) are periodic arrays of nano- and microscale materials that can display striking colors due to Bragg diffraction.[1−5] In contrast to dyes and pigments, which absorb specific wavelengths of light, PCs are resistant to photobleaching, and their color is dependent on the spatial periodicity of the material rather than its chemical composition. As predicted by Bragg's law of diffraction, the specific coloration of PCs can be tuned by adjusting the spacing in the periodic array.[6−9]

The ability to create responsive PC materials that can tune coloration in space and time is highly desirable, as such materials have important applications in sensing,[2,6,8] camouflage,[10,11] and anti-counterfeiting inscriptions.[9,12,13] Most responsive PC materials are generated by embedding or etching PC structures in a hydrogel matrix that displays a volume change (i.e., swelling or collapse) in response to specific types of input.[14,15] These changes in the matrix modulate the lattice constant of the PC and hence tune the color of the material. One of the greatest challenges in this area pertains to the creation of periodic assemblies of nanoparticles within a hydrogel from a disordered array with spatial and temporal control. Herein, we address this challenge and create a PC hydrogel that displays an on-demand coloration by using DNA supramolecular hydrogels that can rapidly and locally switch between crosslinked and de-crosslinked states using an optothermal trigger.

To achieve on-demand assembly with high spatial and temporal resolution, two conditions must be met. (1) A hydrogel must undergo local, reversible, and transient de-crosslinking upon specific inputs, and (2) Nanoparticles should rapidly translocate and organize within the hydrogel during a transient de-crosslinking. To the best of our knowledge, there are no reported examples of nanocomposite hydrogels that meet these conditions. The most commonly adopted approach to form PC hydrogels requires first organizing the PC material using an external magnetic, gravitational, or electric field. Once organized, the hydrogel is crosslinked in a way that the nanoscale periodicity is locked and preserved after the removal of external fields.[3,10,15,16] This is due to the large energy barrier to diffusion created by the hydrogel network, which prevents nanoparticle mobility inside the hydrogel.

Our approach is illustrated in Figure 1 where we used a DNA supramolecular hydrogel[17] constructed from palindromic

Received: September 2, 2021
Revised: October 29, 2021

https://doi.org/10.1021/acs.nanolett.1c03399
Nano Lett. XXXX, XXX, XXX−XXX

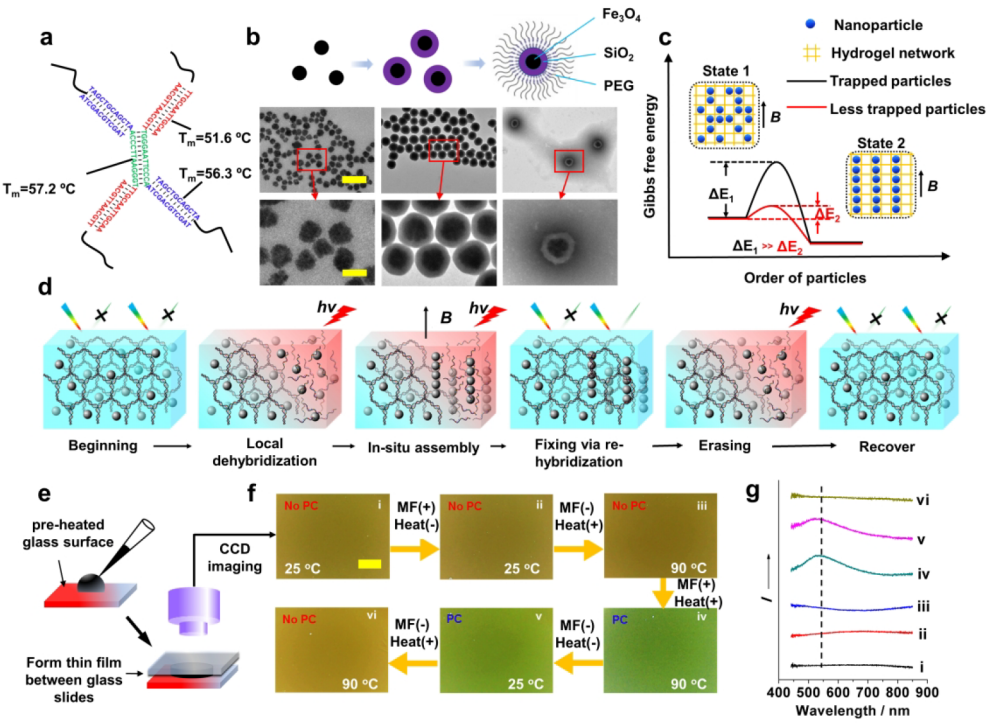

Figure 1. Design and testing of the DNA hydrogel system for on-demand PC patterning and erasing. (a) Design of a purely DNA supramolecular hydrogel system in which the DNA hydrogel is formed from three different palindromic sequence domains located on a single strand. (b) Schematic of MNP synthesis and corresponding TEM images. Magnetite nanoparticles (~120 nm) are coated with a silica shell (~30 nm) first and then a layer of PEG. Scale bar: 500 nm for upper set and 125 nm for lower set. (c) Theoretical energy diagram of in situ assembly of the hydrogel. (d) Mechanism of in situ assembly in which the local and transient dehybridization of a DNA hydrogel would lower the energy barrier for particle assembly under a magnetic field and then regelate to fix the pattern. This can be erased at a later time by dehybridization in the absence of a magnetic field. (e) Schematic of sample preparation and imaging. (f) Digital photographs (states i–vi) of the same hydrogel sample at different conditions showing color changes; the scale bar is 600 μm. (g) Reflectance spectra that correspond to the photographs in (f), displaying the emerging reflectance peak ~530 nm after in situ assembly, which corresponds to the Bragg diffraction of the assembled PC.

single-stranded DNA (ssDNA) with three self-complementary domains (red, green, and blue domains in Figure 1a). To create the PC, we used super-paramagnetic magnetite nanoparticles (MNPs) coated with poly(ethylene glycol) (PEG) that assemble into periodic structures under an external magnetic field (Figure 1b, also see Figure S1 showing TEM images of different sizes of MNPs). PEGylated MNPs are sufficiently stable to assemble in aqueous buffers with a higher ionic strength, which is necessary for DNA hydrogel formation (Figure S2). Given that crosslinks are exclusively created using hybridized DNA strands, denaturing the DNA allows for complete de-crosslinking of the hydrogel and thus lifting of the energy barrier for particle mobility (Figure 1c). In contrast to other supramolecular hydrogels, pure DNA-based hydrogels in this work display faster gelation kinetics with a time resolution of seconds and a relatively rigid network that can hold the in situ assembled structure. These two features are advantageous for on-demand structural coloration and decoloration.

The key design criteria for creating an on-demand PC material are illustrated using a simplified energy diagram in Figure 1c, where the *y*-axis represents the free energy of the system, and the *x*-axis represents an order parameter (e.g., the particle organization). State 1 illustrates an initial condition where particles are randomly distributed inside the hydrogel network, while state 2 represents ordered particles that form the PC. Under the influence of an external magnetic field (B), state 1 is higher in energy compared to state 2 due to the potential energy of the magnetic dipole moments of the MNPs.

In order for the particles to organize, they must overcome the energy barrier required for movement across the DNA hydrogel network. This barrier is large when the DNA is fully hybridized (black curve Figure 1c), and hence particles are locked in place. When the DNA is denatured, the barrier to reach state 2 is lowered and thus allows for particles translocation to occur (red curve, Figure 1c). Figure 1d illustrates the overall cycle of triggered on-demand assembly (patterning) and disassembly (erasing) of the PC within the DNA hydrogel. In our case, we trigger the DNA disassembly using the broad absorption spectrum and high photothermal conversion efficiency of MNPs. This can locally and transiently melt the DNA network and dramatically lower the energy barrier of particle translocation (Figure S3). Simulation of the photothermal effect of the laser on the hydrogel is illustrated in Figure S4, which indicates that the heat generated by MNPs is large enough to dehybridize the surrounding DNA duplex network. Upon illumination, the MNPs generate heat and locally melt the gel as they translocate and align with an external magnetic field, therefore forming a periodic PC structure. Upon removal of the illumination, a rapid heat dissipation results in a rehybridization of DNA strands. This locks the patterned PC in the DNA gel. Notably, these PC patterns can be rapidly "erased" by an illumination in the absence of an external magnetic field.

https://doi.org/10.1021/acs.nanolett.1c03399
Nano Lett. XXXX, XXX, XXX−XXX

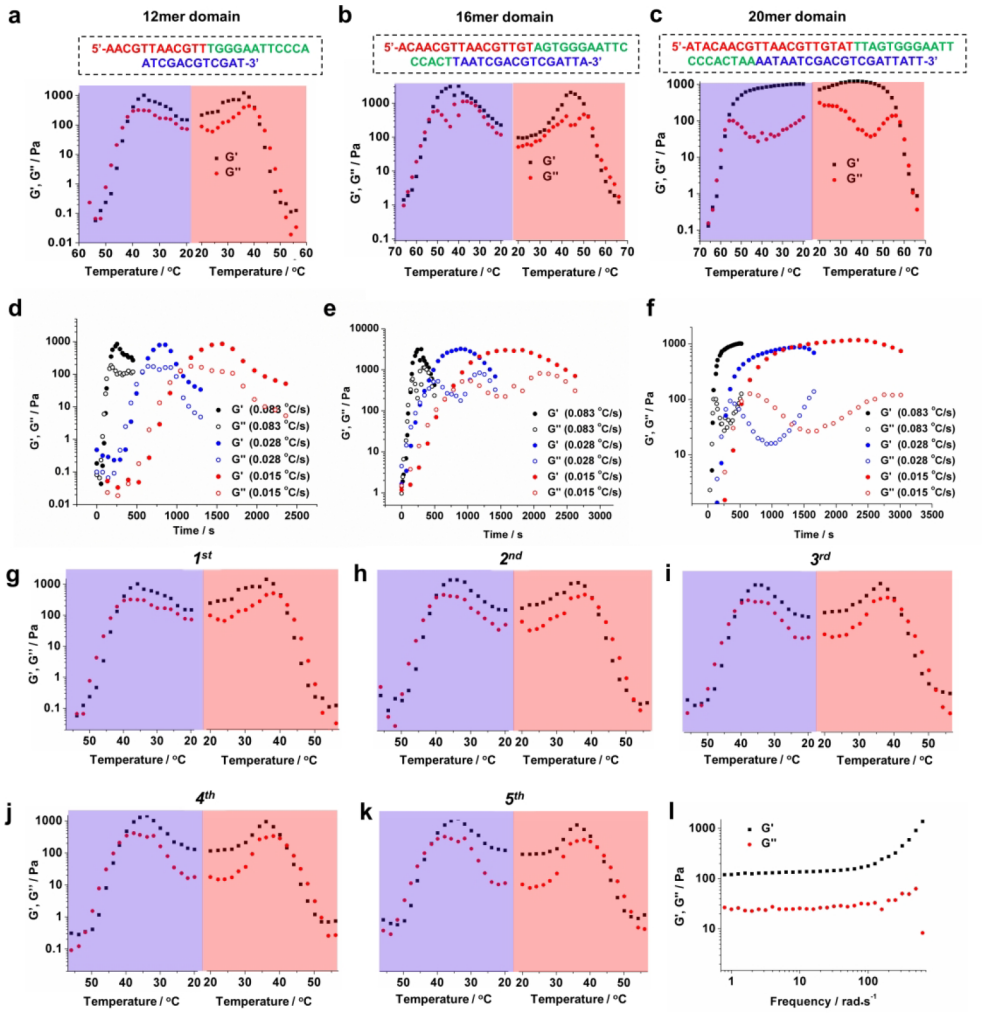

Figure 2. Rheology characterization of DNA supramolecular hydrogel/MNP composites. (a–c) Rheology plots during cooling–heating cycles of PC hydrogels. The DNA supramolecular hydrogel is designed with three different sequences with palindromic domain lengths of (a) 12, (b) 16, and (c) 20 bases. (d–f) Rheology results using different scan rates (0.083, 0.028, and 0.015 °C/s) for different PC hydrogels shown in (a–c). (g–k) The cooling–heating cycles of PC hydrogels formation from 12mer palindromic domain DNA sequence. (l) A frequency scan at room temperature of PC hydrogel formation with 12mer domain DNA strands to test the integrity of the hydrogel ($G' > G''$).

RESULTS AND DISCUSSION

As a proof of concept, we tested our design using bulk heating to drive the DNA denaturation. After mixing the MNP solution with the palindromic ssDNA, we heated the sample to 90 °C in a potassium phosphate buffer (37 mM, pH = 7) to form a homogeneous solution. The solution was cast on a preheated glass surface and then sandwiched using a second glass slide (Figure 1e). A thin film of the mixture was then allowed to cool to room temperature, thus forming a hydrogel (Figure 1f). The formed gel displayed a brown color, and its reflection spectra lacked any clear features (state i in Figure 1f,g).

Neither the physical appearance of the material nor its reflection spectra changed when a magnetic field (~200 G) was applied to the gel (state ii in Figure 1f,g). Likewise no change was observed when the gel was only heated (90 °C) (state iii in Figure 1f,g). However, when the gel was heated (90 °C) while simultaneously applying a magnetic field (~200 G), a green coloration appeared that was consistent with the appearance of a reflection band λ = 530 nm, thus confirming the formation of the PC (state iv in Figure 1f,g). The PC was maintained even after the sample was cooled to room temperature (state v in Figure 1f,g). Notably, heating the sample without applying an external magnetic field disrupted the structural color and allowed the material to return to its original non-PC (brown color) state (state vi in Figure 1f,g). These results support the model described in Figure 1d and suggest the feasibility of reversible patterning of the PC with a photothermal input.

To better understand the gelation behavior of the DNA photonic hydrogel, we next performed rheology measurements as a function of DNA sequence, gelation time, and temperature. First, three different sequences were designed and used to create DNA/nanoparticle composite hydrogels. Each sequence contained three palindromic domains of increasing length, 12, 16, and 20 oligomers (Figure 2a–c). Figure 2a–c shows that gelation was reversible within a single cooling (purple) and heating (red) cycle. At elevated temperatures, all samples were in a low-viscosity liquid state as G' was similar to G'', and their values were fairly low. As the temperature dropped, DNA hybridization proceeds; this leads to gelation of the material as indicated with a drastic increase in G' and G'', and $G' > G''$. The apparent peak in G' and G'' is likely due to the volume change in the hydrogel due to hybridization.[18] We

https://doi.org/10.1021/acs.nanolett.1c03399
Nano Lett. XXXX, XXX, XXX–XXX

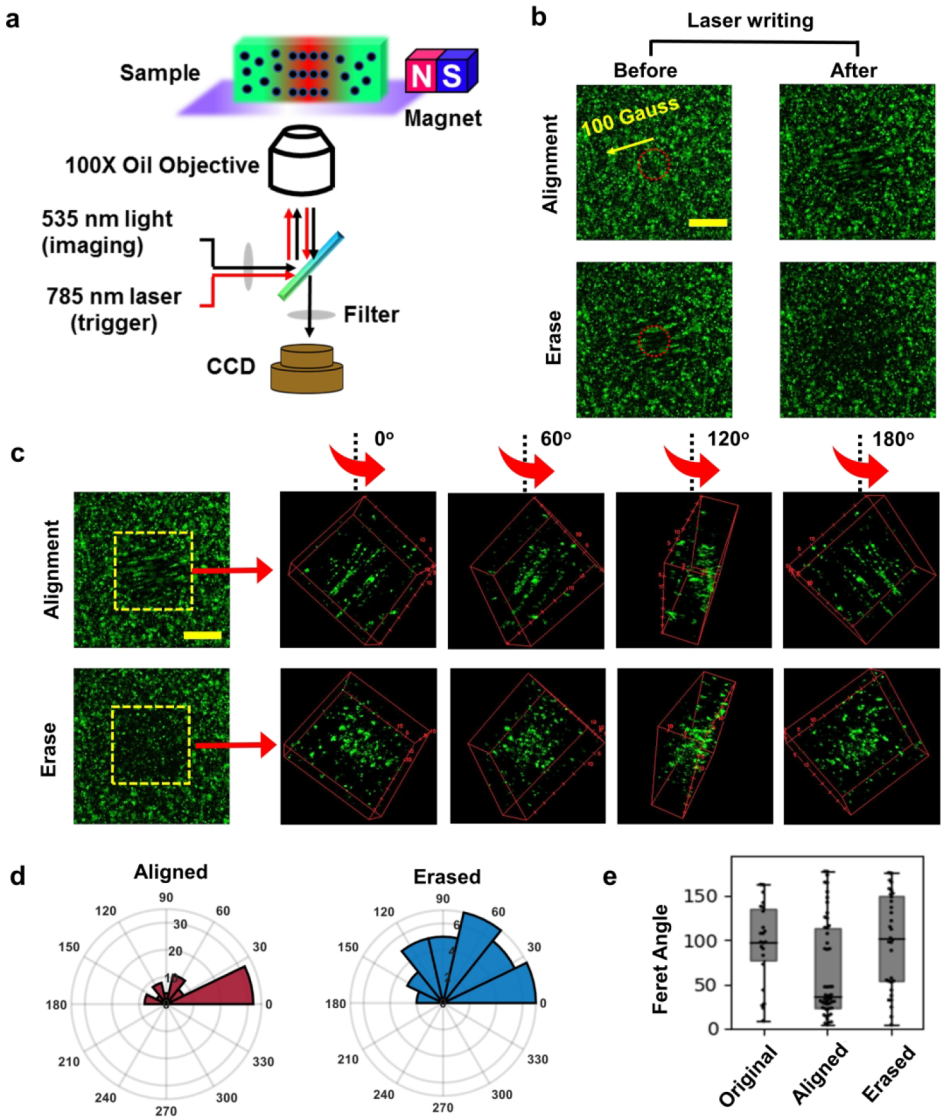

Figure 3. Microscopic imaging results of on-demand assembly. (a) Schematic of microscope settings for in situ imaging. The sample was on a glass slide and observed by a 100× oil objective with an optical path to a CCD camera and 785 nm laser controlled by a galvo-mirror system for spatially selective excitation. (b) Comparison of nanopattern changes inside the hydrogel before and after laser irradiation was applied. (upper set) Laser writing of PC nanopatterns. (lower set) Laser erasing of PC nanopatterns. Scale bar: 20 μm. (c) 3D reconstructed images based on z-scans of the sample at different angles of rotation demonstrating organized or disorganized structures inside the hydrogel. Scale bar: 20 μm. (d) Feret angles plotted in histogram based on a statistical analysis of aligned or erased structures that correspond to an automated object detection ridge analysis of sample images. (e) Box plot shows the statistical analysis of Feret angles measured from original, aligned, or erased samples.

also synthesized two additional sizes of MNPs to test the influence of particle size on the rheology of the hydrogel. We did not find a significant difference in rheology for DNA hydrogels embedded with 140, 180, and 200 nm diameter MNPs (Figure S5).

To investigate the effect of DNA sequence on gelation kinetics, we performed time-dependent rheology measurements. In principle, longer sequences should display slower hybridization kinetics and hence longer gelation times. Surprisingly, rheology measurements showed nearly identical gelation kinetics for the three sequences (Figure 2d–f). This is likely because the gelation time of the DNA is rapid and proceeds at time scales exceeding the time resolution of the rheometer (~0.083 °C/s). Thus, this indicates that the palindromic DNA gelation kinetics are fast, which is advantageous to achieve our goal of an on-demand formation of PC structure.

In order to test the reversible gelation behavior, we additionally performed rheology measurements while we ran multiple thermal cycles on the DNA composite hydrogel formed by the 12-mer domain (Figure 2g–k). We found that the gelation behavior does not significantly change even after five heating–cooling cycles and that the sample showed classic hydrogel behavior ($G' > G''$) at room temperature following thermal cycling. These results confirm the possibility of generating erasable PC patterns by a repeated thermal cycling of the DNA hydrogels.

Figure 2l shows a plot of the G' and G'' as a function of frequency at room temperature. The data confirm that $G' > G''$ across the tested frequencies showing classic hydrogel behavior. We were unable to plot G' and G'' above the transition temperature, as the gel was completely liquid and displayed the minimum G' and G'' reportable values of ~0.02 Pa, which is the limit of the rheometer resolution. These

https://doi.org/10.1021/acs.nanolett.1c03399
Nano Lett. XXXX, XXX, XXX−XXX

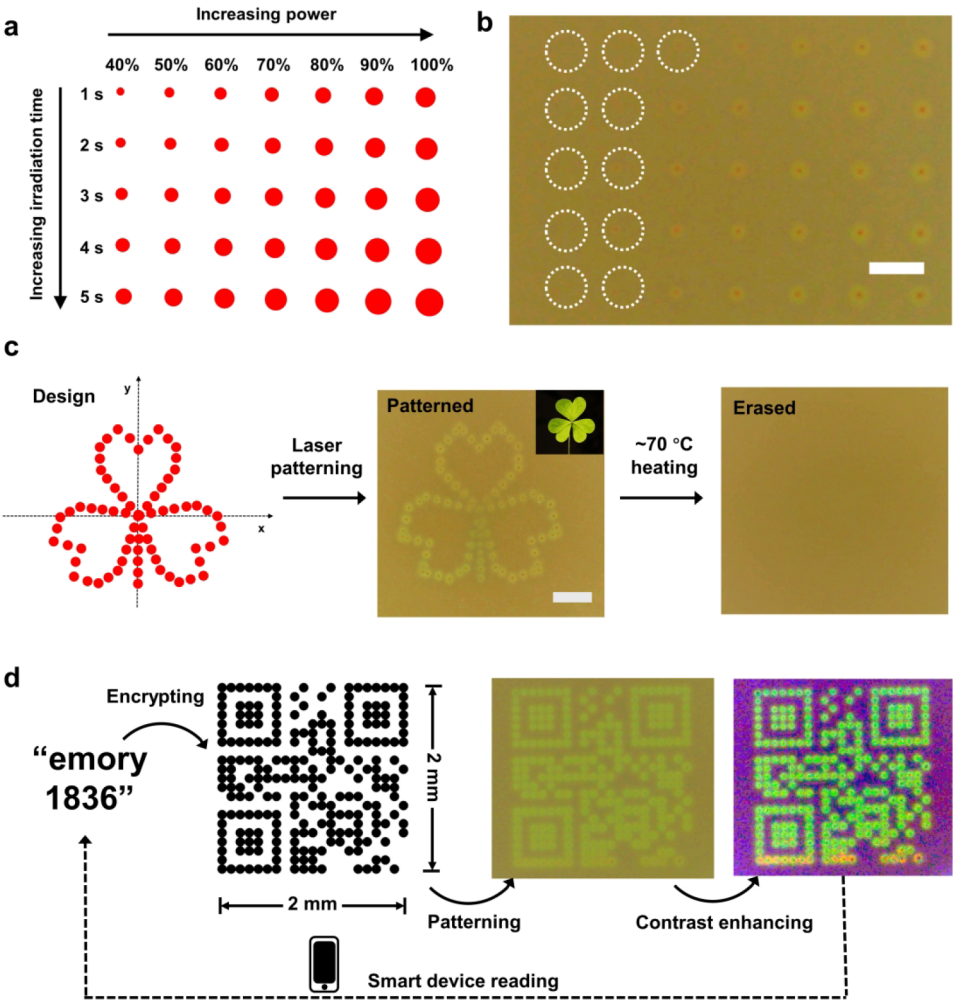

Figure 4. Laser-patterning demonstrations of in situ assembly of DNA supramolecular hydrogels. (a) Laser-patterning map based on different laser power and laser irradiation times. Note that 100% laser power is ~49.7 mW. (b) Digital photograph of the laser-patterned spots based on the design of (a) (scale bar 300 μm). (c) A laser-patterning design of a three-leaf clover after the patterning and the real image (top inset). The patterned image can be erased by a bulk heating. Scale bar 400 μm. (d) A flow diagram demonstrates an encrypting application of an on-demand assembly. A QR code that encrypted the text Emory 1836 was generated first by software. Then, we photopatterned the QR code (2 mm × 2 mm) with the on-demand assembly technology in this work. After the contrasts of the microscope image were adjusted, the QR code was read by a smart device to reveal the encrypted information. Note: All hydrogels were imaged at room temperature in the absence of a magnetic field.

palindromic DNA hydrogels are rheologically distinct from hybrid gels comprised of acrylamide polymers crosslinked using DNA. The rheology measurements for the acrylamide-DNA gels showed a relatively high G' above the transition temperature, which is likely due to the entanglement of its long polymer backbone (Figure S6). Therefore, acrylamide-DNA gels would still significantly hinder the reorganization of MNPs above the transition temperature so that on-demand assembly of PC would fail (Figure S7). Hence, this particular three-domain palindromic DNA offers properties that are advantageous for the goal of on-demand assembly of PC structures.

To provide further evidence of light- and magnetic-field-driven assembly of the MNPs into a PC structure within the DNA hydrogel, we employed high-resolution optical microscopy to observe the microscopic assembly of the particles. In our microscope setup, we observed the MNPs by using reflection interference contrast microscopy (RICM) at λ_{ex} = 535 nm while simultaneously exciting the region of interest using a galvo-controlled ~5 μm diameter 785 nm laser irradiation system (Figure 3a). We used a rare-earth magnet to generate a magnetic field (~100 G) that drives the assembly of MNPs in a direction that is parallel to the magnetic field and the observation plane. Figure 3b shows RICM images displaying the organization of the MNPs prior to and after near-IR illumination (785 nm) for 10 s (red circle; duty cycle 50%; power = 36.2 mW; on-time = 500 ms). We note the formation of linear assemblies of particles that align with the external magnetic field. To demonstrate the reversibility of the PC assembly, we next illuminated the same region for another 10 s (red circle; duty cycle 50%; power = 36.2 mW; on-time = 500 ms) in the absence of the magnetic field. The bottom two images in Figure 3b show the loss of particle organization in the absence of the external magnetic field. Importantly, the particle assembly was confined to the near-IR illumination area, while the remaining regions showed static particles that remained randomly distributed (Supporting Information, Videos 1 and 2; also see Videos 3 and 4 for patterning with a different direction of magnetic field on a single piece of hydrogel). Similar results were also found in DNA hydrogels with the 140 and 200 nm diameter MNPs (Figure S8). We also

https://doi.org/10.1021/acs.nanolett.1c03399
Nano Lett. XXXX, XXX, XXX−XXX

performed z-stack scanning in the RICM channel and generated three-dimensional (3D) reconstruction images (in ImageJ) to further identify the linear assemblies of MNPs inside the gel after an alignment where the MNPs assemblies are erased (Figure 3c). Quantitative analyses of the alignment were conducted using the ridge detection plugin[19] of ImageJ (Figure S9), which allowed us to measure an in-plane Feret angle for the linear assemblies using the microscope image frame of reference where $\theta = 0°$, which is parallel to the x-axis and serves as the frame of reference. Figure 3d,e shows radial histograms and box plots, respectively, that were collected from three regions of interest after the alignment and erasing of the linear assemblies as described above. In Figure 3d, the fan area indicates the angle distribution. The largest area from the Feret angle of the aligned MNPs was the area that represents 0−30°, coinciding with the approximate direction of the magnetic field (as illustrated in Figure 3b). After the erasure, the angle preference was lost, since other fan areas grow nearly as large as the one that represents 0−30°. In box plots (Figure 3e), the data points of the original sample showed a uniform distribution span from 0 to 180°. However, most of the data points converge to ∼30° after the alignment, which indicates an angle of interest that is similar to that of Figure 3d. This alignment is lost again in the box plot that represents the erased sample. To summarize, the laser- and magnetic-field-induced on-demand patterning is effective and swift as expected.

On-demand and in situ assembly of PC structures in hydrogels has many potential applications. One of these applications is for on-demand writing/erasing, which was described recently.[20−22] To demonstrate this potential application using our approach, we conducted a series of writing/erasing tests in the DNA hydrogel samples. As described above, photothermal heating can trigger a local melting of the DNA, thus minimizing the energy barrier of the MNP translocation and allowing for on-demand assembly. Our first goal was to quantify how the irradiation time and power tune the local assembly and coloration of the PC gel. Hence we designed an array of irradiation spots with different laser powers (40%−100%) and irradiation times (1−5 s) and captured images of the gel before and after an illumination (Figure 4a). The experiment was conducted under an external magnetic field that was perpendicular to the observation plane. We found that the color of the PC gel did not change when the total input energy was low, when the illumination time was brief, or if the illumination intensity was weak (e.g., 40% laser power, 1 s of irradiation time). At greater illumination intensities and dwell times, we observed that the diameter of the spots increased as a function of the energy input (Figure 4b). This is likely due to the accumulation of heat allowing for the melting of greater regions of DNA and the migration of greater numbers of MNPs from the surrounding hydrogel. We also observed the formation of spots that seemed to have a colored ring and dark center. According to our investigation, the dark center is likely due to the depletion of DNA because the hydrogel unevenly redistributed after being heated/cooled (Figure S10). This is supported by control experiments using fluorophore-labeled ssDNA (Figure S11). We also found that a laser power of 80% with 3 s of irradiation time produced optimal results, since the spot size produced sufficient contrast from the background and the spot size was smaller suggesting an improvement in the spatial resolution. Additionally, the spot size is related to particle concentration. The melting area changed drastically when we photothermally heated the hydrogel sample. This is due to the higher particle concentration for the samples with a greater weight percent, which produces greater amounts of heat upon illumination (Figure S12). By applying this protocol using patterns with preassigned (x,y) coordinates, we first created a three-leaf clover-like figure with an area of 1−2 mm^2, which was spatially patterned and erased after the bulk was heated and cooled (Figure 4c, also see the Supporting Information, Video 5). We also demonstrated the patterning of a quick response (QR) code (2 mm × 2 mm) that was encrypted with the text information "Emory 1836" in Figure 4d. The information can be stored and later read using a smart device (Supporting Information, Video 6) as we showed in this figure. In our system, this pattern was comprised of ∼250 spots and required ∼10 min to complete with a single laser illumination system, thus demonstrating the ability to create patterns on-demand. Compared to rewritable technology based on photochromic materials,[22,23] our method is free of photobleaching, does not require a photomask, and generates patterns more rapidly.

CONCLUSION

In summary, we demonstrate an on-demand structural color patterning technology using a DNA supramolecular hydrogel system with high spatial and temporal resolution. The gel is crosslinked using all noncovalent Watson−Crick−Franklin interactions, which are advantageous because these can be easily programmed. The self-assembly of MNPs created PC structural color that could be controlled and erased on demand based on specific thermal, optical, and magnetic inputs. Rheology measurements of the hydrogel composite show highly reversible and rapid crosslinking/de-crosslinking kinetics, which were observed for the three palindromic DNA sequences tested (12, 16, and 20 mer domains). The generation of PC coloration required transient de-crosslinking of the gel with a simultaneous application of an external magnetic field to assemble the MNP. This coloration was rapidly erased when the gels were transiently de-crosslinked in the absence of a magnetic field. Because of the strong visible and near-IR absorbance of the MNPs, the structural color could be patterned in a facile manner using a near-IR laser source with micrometer spatial resolution and subsecond temporal resolution. It is important to note that many reported examples of rewritable materials are based on organic dye,[22,24,25] PC,[26−28] and metal−organic framework (MOF)[29] materials. In contrast to organic dye materials, PCs offer a more stable coloration that resists photobleaching and degradation that are well-documented for organic dyes and pigments. Other PC-rewritable approaches display slow response times (for writing and erasing), as these systems require a volumetric swelling/deswelling change in the polymer matrix. For example, water-triggered reversible PC coloration required ∼5−10 min response times.[26] By leveraging the rapid and highly localized gelation/degelation kinetics of palindromic DNA, our strategy offers high spatial resolution (up to ∼10 μm), direct-write color patterning without the need for a photomask, and rapid patterning (<1 s) and erasing (<10 s). Supporting Information Table 1 compares some of the reported technologies to generate rewritable materials. Finally, we note that the fundamental strategy disclosed here might inspire other applications such as chemical sensing, molecular diagnostics, and information

https://doi.org/10.1021/acs.nanolett.1c03399
Nano Lett. XXXX, XXX, XXX−XXX

storage due to the programmability and sensitivity of DNA-based hydrogels.

■ ASSOCIATED CONTENT

Supporting Information

The Supporting Information is available free of charge at https://pubs.acs.org/doi/10.1021/acs.nanolett.1c03399.

Experimental section, characterization, reflection spectra of nanoparticle assembly, TEM images with different sizes of MNPs, proof-of-concept experiment for photothermal dehybridization, finite element simulation of photothermal effect of MNPs, rheology test for DNA duplex crosslinked polyacrylamide hydrogel, microscope images of attempted particle realignment in synthetic polymer hydrogel crosslinked by DNA duplex, examples of ridge detection, fluorescence microscope images (PDF)

Supplementary video 1 (AVI)

Supplementary video 2 (AVI)

Supplementary video 3 (AVI)

Supplementary video 4 (AVI)

Supplementary video 5 (AVI)

Supplementary video 6 (MP4)

■ AUTHOR INFORMATION

Corresponding Author

Khalid Salaita − *Department of Chemistry, Emory University, Atlanta, Georgia 30322, United States;* orcid.org/0000-0003-4138-3477; Email: k.salaita@emory.edu

Authors

Yixiao Dong − *Department of Chemistry, Emory University, Atlanta, Georgia 30322, United States;* orcid.org/0000-0001-8943-9842

J. Dale Combs − *Department of Chemistry, Emory University, Atlanta, Georgia 30322, United States*

Cong Cao − *Department of Physics, Emory University, Atlanta, Georgia 30322, United States*

Eric R. Weeks − *Department of Physics, Emory University, Atlanta, Georgia 30322, United States;* orcid.org/0000-0003-1503-3633

Alisina Bazrafshan − *Department of Chemistry, Emory University, Atlanta, Georgia 30322, United States;* orcid.org/0000-0002-3259-8196

SK Aysha Rashid − *Department of Chemistry, Emory University, Atlanta, Georgia 30322, United States*

Complete contact information is available at: https://pubs.acs.org/10.1021/acs.nanolett.1c03399

Author Contributions

Y.D. and K.S. conceived of the project. Y.D. designed and performed most of the experiments. J.D.C. helped with the in situ imaging, statistical analysis, and related discussions. C.C. and E.R.W. helped with rheological experiments and related discussions. A.B. helped with proof-of-concept experiments. S.K.A.R. helped with the laser-patterning demonstration. K.S. and Y.D. wrote the manuscript. All the authors helped revise the manuscript.

Notes

The authors declare no competing financial interest.

■ ACKNOWLEDGMENTS

This work is supported by NSF DMR 1905947, NIH R01 GM 131099 and NIH R01 GM 124472. The authors especially thank Dr. Y. Ke from the department of biomedical engineering at Emory University for his three-domain ssDNA design.

■ REFERENCES

(1) Yang, Y.; Chen, Y.; Hou, Z.; Li, F.; Xu, M.; Liu, Y.; Tian, D.; Zhang, L.; Xu, J.; Zhu, J. Responsive Photonic Crystal Microcapsules of Block Copolymers with Enhanced Monochromaticity. *ACS Nano* **2020**, *14* (11), 16057−16064.

(2) Chen, Q.; Wang, C.; Wang, S.; Zhou, J.; Wu, Z. A responsive photonic crystal film sensor for the ultrasensitive detection of uranyl ions. *Analyst* **2020**, *145* (16), 5624−5630.

(3) Ge, J.; Yin, Y. Responsive photonic crystals. *Angew. Chem., Int. Ed.* **2011**, *50* (7), 1492−1522.

(4) Yue, Y.; Kurokawa, T. Designing responsive photonic crystal patterns by using laser engraving. *ACS Appl. Mater. Interfaces* **2019**, *11* (11), 10841−10847.

(5) Yang, B.; Li, L.; Du, K.; Fan, B.; Long, Y.; Song, K. Photo-responsive photonic crystals for broad wavelength shifts. *Chem. Commun.* **2018**, *54* (24), 3057−3060.

(6) Cai, Z.; Sasmal, A.; Liu, X.; Asher, S. A. Responsive photonic crystal carbohydrate hydrogel sensor materials for selective and sensitive lectin protein detection. *ACS sensors* **2017**, *2* (10), 1474−1481.

(7) Chen, H.; Hou, A.; Zheng, C.; Tang, J.; Xie, K.; Gao, A. Light- and humidity-responsive chiral nematic photonic crystal films based on cellulose nanocrystals. *ACS Appl. Mater. Interfaces* **2020**, *12* (21), 24505−24511.

(8) Zhang, J.-T.; Wang, L.; Luo, J.; Tikhonov, A.; Kornienko, N.; Asher, S. A. 2-D array photonic crystal sensing motif. *J. Am. Chem. Soc.* **2011**, *133* (24), 9152−9155.

(9) Hu, H.; Chen, Q.-W.; Tang, J.; Hu, X.-Y.; Zhou, X.-H. Photonic anti-counterfeiting using structural colors derived from magnetic-responsive photonic crystals with double photonic bandgap heterostructures. *J. Mater. Chem.* **2012**, *22* (22), 11048−11053.

(10) Dong, Y.; Bazrafshan, A.; Pokutta, A.; Sulejmani, F.; Sun, W.; Combs, J. D.; Clarke, K. C.; Salaita, K. Chameleon-inspired strain-accommodating smart skin. *ACS Nano* **2019**, *13* (9), 9918−9926.

(11) Moirangthem, M.; Schenning, A. P. Full color camouflage in a printable photonic blue-colored polymer. *ACS Appl. Mater. Interfaces* **2018**, *10* (4), 4168−4172.

(12) Chen, K.; Zhang, Y.; Ge, J. Highly invisible photonic crystal patterns encrypted in an inverse opaline macroporous polyurethane film for anti-counterfeiting applications. *ACS Appl. Mater. Interfaces* **2019**, *11* (48), 45256−45264.

(13) Hu, H.; Zhong, H.; Chen, C.; Chen, Q. Magnetically responsive photonic watermarks on banknotes. *J. Mater. Chem. C* **2014**, *2* (19), 3695−3702.

(14) Goodling, A. E.; Nagelberg, S.; Kolle, M.; Zarzar, L. D. Tunable and responsive structural color from polymeric microstructured surfaces enabled by interference of totally internally reflected light. *ACS Materials Letters* **2020**, *2* (7), 754−763.

(15) Jia, X.; Xiao, T.; Hou, Z.; Xiao, L.; Qi, Y.; Hou, Z.; Zhu, J. Chemically Responsive Photonic Crystal Hydrogels for Selective and Visual Sensing of Thiol-Containing Biomolecules. *ACS omega* **2019**, *4* (7), 12043−12048.

(16) Liu, F.; Zhang, S.; Jin, X.; Wang, W.; Tang, B. Thermal-Responsive Photonic Crystal with Function of Color Switch Based on Thermochromic System. *ACS Appl. Mater. Interfaces* **2019**, *11* (42), 39125−39131.

(17) Jiang, H.; Pan, V.; Vivek, S.; Weeks, E. R.; Ke, Y. Programmable DNA hydrogels assembled from multidomain DNA strands. *ChemBioChem* **2016**, *17* (12), 1156−1162.

(18) Topuz, F.; Okay, O. Rheological behavior of responsive DNA hydrogels. *Macromolecules* **2008**, *41* (22), 8847−8854.

(19) Steger, C. An unbiased detector of curvilinear structures. *IEEE Transactions on pattern analysis and machine intelligence* **1998**, *20* (2), 113−125.
(20) Chen, C.; Zhao, X.; Chen, Y.; Wang, X.; Chen, Z.; Li, H.; Wang, K.; Zheng, X.; Liu, H. Reversible Writing/Re-Writing Polymeric Paper in Multiple Environments. *Adv. Funct. Mater.* **2021**, *31*, 2104784.
(21) Chen, L.; Weng, M.; Huang, F.; Zhang, W. Long-lasting and easy-to-use rewritable paper fabricated by printing technology. *ACS Appl. Mater. Interfaces* **2018**, *10* (46), 40149−40155.
(22) Müller, V.; Hungerland, T.; Baljozovic, M.; Jung, T.; Spencer, N. D.; Eghlidi, H.; Payamyar, P.; Schlüter, A. D. Ink-Free Reversible Optical Writing in Monolayers by Polymerization of a Trifunctional Monomer: Toward Rewritable "Molecular Paper. *Adv. Mater.* **2017**, *29* (27), 1701220.
(23) Khazi, M. I.; Jeong, W.; Kim, J. M. Functional materials and systems for rewritable paper. *Adv. Mater.* **2018**, *30* (15), 1705310.
(24) Wei, J.; Jiao, X.; Wang, T.; Chen, D. Electrospun photochromic hybrid membranes for flexible rewritable media. *ACS Appl. Mater. Interfaces* **2016**, *8* (43), 29713−29720.
(25) Wu, H.; Chen, Y.; Liu, Y. Reversibly photoswitchable supramolecular assembly and its application as a photoerasable fluorescent ink. *Adv. Mater.* **2017**, *29* (10), 1605271.
(26) Du, X.; Li, T.; Li, L.; Zhang, Z.; Wu, T. Water as a colorful ink: transparent, rewritable photonic coatings based on colloidal crystals embedded in chitosan hydrogel. *J. Mater. Chem. C* **2015**, *3* (15), 3542−3546.
(27) Wang, M.; He, L.; Hu, Y.; Yin, Y. Magnetically rewritable photonic ink based on superparamagnetic nanochains. *J. Mater. Chem. C* **2013**, *1* (38), 6151−6156.
(28) Ge, J.; Goebl, J.; He, L.; Lu, Z.; Yin, Y. Rewritable photonic paper with hygroscopic salt solution as ink. *Adv. Mater.* **2009**, *21* (42), 4259−4264.
(29) Garai, B.; Mallick, A.; Banerjee, R. Photochromic metal−organic frameworks for inkless and erasable printing. *Chem. Sci.* **2016**, *7* (3), 2195−2200.

https://doi.org/10.1021/acs.nanolett.1c03399
Nano Lett. XXXX, XXX, XXX−XXX